Cite as: A. H. Ghadimi *et al.*, *Science* 10.1126/science.aar6939 (2018).

Elastic strain engineering for ultralow mechanical dissipation

A. H. Ghadimi,[1]* S. A. Fedorov,[1]* N. J. Engelsen,[1]* M. J. Bereyhi,[1] R. Schilling,[1] D. J. Wilson,[2]† T. J. Kippenberg[1]†

[1]Institute of Physics, École Polytechnique Fédérale de Lausanne, 1015 Lausanne, Switzerland. [2]IBM Research–Zurich, 8803 Rüschlikon, Switzerland.

*These authors contributed equally to this work.

†Corresponding author. Email: daw@zurich.ibm.com (D.J.W.); tobias.kippenberg@epfl.ch (T.J.K.)

Extreme stresses can be produced in nanoscale structures, a feature which has been used to realize enhanced materials properties, such as the high mobility of silicon in modern transistors. Here we show how nanoscale stress can be used to realize exceptionally low mechanical dissipation, when combined with "soft-clamping" — a form of phononic engineering. Specifically, using a non-uniform phononic crystal pattern, we colocalize the strain and flexural motion of a free-standing Si_3N_4 nanobeam. Ringdown measurements at room temperature reveal string-like modes with quality (Q) factors as high as 800 million and $Q \times$ frequency exceeding 10^{15} Hz. These results illustrate a promising route for engineering ultra-coherent nanomechanical devices.

Elastic strain engineering (ESE) utilizes stress to realize unusual material properties (*1*). For instance, stress can be used to enhance the electron mobility of a semiconductor, enabling more efficient solar cells (*2*) and smaller, faster transistors (*3*). In mechanical engineering, the pursuit of resonators with low dissipation (*4*) has led to study of a complementary strain engineering technique, "dissipation dilution", whereby the stiffness of a stressed material is effectively increased without added loss (*5–8*). Unlike most bulk mechanical properties, dissipation dilution can improve with reduced device dimensions, implying that smaller mass resonators can have higher Q. This unusual scaling is responsible for the anomalously high Q of Si_3N_4 nanomechanical resonators (*8–11*), including the emergence of quantum coherent resonators, possessing a thermal decoherence time $\hbar Q/k_B T$ larger than one vibrational period (where $\hbar$, k_B, and T are the reduced Planck's constant, Boltzmann constant, and bath temperature, respectively).

Whereas ESE commonly relies on extreme inhomogeneous stresses produced by nanoscale deformation (*12*) (e.g., by lithographic patterning (*13*, *14*) or nano-indentation (*15*)), nearly all studies of dissipation dilution have focused on materials under weak, uniform stress produced during material synthesis. The main challenge in bridging these two approaches is to identify strategies to colocalize stress and mechanical motion at the nanoscale. Our strategy, based on phononic crystal patterning, is conceptually simple and entirely material independent (Fig. 1): By weakly corrugating a prestressed nanobeam, we create a bandgap for localizing its flexural modes around a central defect. By tapering the beam, we colocalize these modes with a region of enhanced stress. Reduced motion near the supports ("soft-clamping" (*8*)) results in higher dissipation dilution, while enhanced stress increases both dilution and mode frequency. Leveraging a multi-step release process, we implement our approach on extremely high aspect ratio tapered beams (as long as 7 mm and as thin as 20 nm) made of prestressed (1.1 GPa) Si_3N_4, and achieve local stresses as high as 3.8 GPa.

We first consider a model for dissipation dilution of a non-uniform beam of length L, thickness h and variable width $w(x)$. Following an anelastic approach successfully applied to uniform nanobeams (*6*, *7*) and nanomembranes (*16*), we partition the potential energy of the beam U into two components: a dissipative component due to bending, $U_E = \frac{1}{2} E_0 \int_0^L I(x)\left[u''(x)\right]^2 dx$, and a conservative component due to elongation, $U_\sigma = \frac{1}{2} T \int_0^L \left[u'(x)\right]^2 dx$, where $u(x)$ is the vibrational modeshape and $I(x) = (1/12)w(x)h^3$, $T = hw(x)\sigma(x)$ and $\sigma(x)$ are the geometric moment of inertia, tension, and axial stress of the beam, respectively. The Q enhancement due to stress (the dissipation "dilution factor") is given by the participation ratio of the lossy potential (*5–7*):

$$\frac{Q}{Q_0} = 1 + \frac{U_\sigma}{U_E} \approx \frac{12}{E_0 h^2} \cdot \frac{\int_0^L \left[u'(x)\right]^2 dx}{\int_0^L \sigma^{-1}(x)\left[u''(x)\right]^2 dx} \quad (1)$$

where Q_0 is the intrinsic (undiluted) quality factor. For the familiar case of a uniform beam with string-like modeshape $u(x) \propto \sin(\pi n x/L)$, Eq. 1 implies that

$$\frac{Q}{Q_0} \approx \frac{3}{\pi^2} \frac{\sigma^2}{E_0 h^2 \rho f^2} \quad (2)$$

where ρ is the material density and $f = \frac{n}{L}\sqrt{\sigma/\rho}$ is the mode frequency. Nearly all stressed nanomechanical resonators studied to date have operated far below this limit. The main reason for this discrepancy is clamping loss, e.g., for a doubly-clamped beam, boundary conditions $u'(x_0) = u(x_0) = 0$ require that the vibrational modeshape exhibit extra curvature ($u''(x)$) near the supports ($x_0 = 0, L$), resulting in a reduced dilution factor of the form (*7*, *17*)

$$\frac{Q}{Q_0} \approx \left(\underbrace{2\lambda}_{\text{supports}} + \underbrace{\pi^2 n^2 \lambda^2}_{\text{antinodes}} \right)^{-1} \quad (3)$$

where $\lambda = \frac{h}{L}\sqrt{1/12\varepsilon}$ in units of axial strain $\varepsilon = \sigma/E$.

The uniform beam model (Eq. 3) gives several rules of thumb for maximizing the Q or $Q \times f$ of a stressed nanomechanical resonator, namely, Q is typically highest for the fundamental mode ($n = 1$) and can be increased by increasing aspect ratio (L/h) or stress. By contrast, $Q \times f$ is typically larger for high order modes. Both strategies have been explored for a wide variety of beam and membrane-like geometries (*17*, *18*). A third approach, recently demonstrated with a membrane (*8*), is to use periodic micropatterning (a phononic crystal (PnC)) to localize the modeshape away from the supports. By this "soft-clamping" approach, the leading term in Eq. 3 can be suppressed, giving access to the performance of an ideal clamp-free resonator (Eq. 2).

Complementary to soft-clamping, our approach consists of colocalizing the modeshape with a region of geometrically-enhanced stress, making use of the tension balance relation, $\sigma(x) = T/(w(x)h)$ (similar to microbridge structures (*13*, *14*)). Inhomogeneous stress has been exploited in the past to increase the $Q \times f$ of a nanomechanical resonator (*19*); however, performance was in this case limited by rigid clamping. Combining it with soft-clamping can lead to improved performance: For example, Eq. 2 suggests that the Q (for a fixed f) of a typical 1 GPa prestressed Si_3N_4 nanobeam can be enhanced by a factor of 50 before the stress in the thinnest part of the beam reaches the yield strength of Si_3N_4 ($\sigma_{yield} \approx 6$ GPa). This material limit, described by Eq. 2 with $\sigma = \sigma_{yield}$ and illustrated by the hatched region in Fig. 1, can be shown to apply to an arbitrary beam profile $w(x)$ (See supplementary materials (*20*)). In gaining access to it, the main caveat of our approach is the small area in which the stress is enhanced, which implies that high order flexural modes must be used to achieve sufficient colocalization.

Devices were patterned on 20-nm-thick films of high-stress Si_3N_4 ($E_0 \approx 250$ GPa, $\sigma_0 \approx 1.1$ GPa) grown by low pressure chemical vapor deposition on a Si wafer. A multi-step release process (*20*) was used to suspend beams as long as 7 mm, enabling aspect ratios as high as 3.5×10^5 and dilution factors in excess of $(2\lambda)^{-1} \approx 3 \times 10^4$. To realize PnCs, beams were corrugated with a simple step-like unit cell (length L_c, minor width w_{min}, major width $w_{max} \approx 2w_{min}$ (Fig. 2A). A uniform defect of length L_d was patterned at the center of each beam in order to define the position of localized modes. To colocalize stress with these modes, the width of successive unit cells is adiabatically tapered toward the defect according to a Gaussian envelope function (*20*).

Localized modes of PnC nanobeams ("1D phononic crystals") have already been widely studied, as their ultra-low-mass and sparse mode spectrum makes them highly promising for sensing applications. In contrast to 2D (membrane-like) resonators (*8*), however, ultra-high-Q in 1D PnCs has not been reported to date, due to a focus on unstrained materials (*21*), and/or highly-confined (high curvature) modes (*18*) limited by radiation loss. With this discrepancy in mind, we first embarked on a study of uniform (untapered) PnC nanobeams, focusing on localized modes of our high-aspect-ratio devices.

An experiment demonstrating soft-clamped 1D nanomechanical resonators is presented in Fig. 3. 2.6-mm-long devices with unit cells of length $L_c = 100$ μm and width $w_{min(max)} = 0.5(1)$ μm were studied. To characterize these devices, thermal noise and ringdown measurements were carried out in vacuo (<10^{-6} mbar) using a custom lensed fiber interferometer (*20*). As a consequence of their simple geometry, mode frequencies (inferred from thermal noise spectra, Fig. 3E) were found to agree well with a numerical solution to the 1D Euler-Bernoulli (E-B) equation (*20*). Particularly striking is the sparse mode spectrum inside the bandgap, visualized by compiling spectra of beams with different defect lengths (Fig. 3F). A single defect mode appears to move in and out of the bandgap as the defect length is varied. This mode is expected to be localized and to therefore have

a reduced effective mass, m. Comparing the area under thermal noise peaks and estimating the physical beam mass to be m_0 = 100 pg, we infer that indeed $m \approx 5$ pg << m_0 (*20*). This value is in good agreement with the mode profile obtained from the E-B equation (Fig. 3G), and is roughly 2 orders of magnitude smaller than that of an equivalent 2D localized mode.

In accordance with Eq. 3, we also observe a dramatic increase in the Q of localized modes. To visualize this enhancement, we compiled measurements of Q versus mode frequency for 40 beams of different defect length (Fig. 3G). Outside the bandgap, we find that $Q(f)$ is consistent with that of a uniform beam, asymptoting at low mode order (n < ~20) to $Q \approx 2 \times 10^7$, implying $Q_0 \approx 2\lambda Q \approx 1500$. Inside the bandgap ($n \approx 26$), Q approaches that of an idealized clamp-free beam ($Q \approx Q_0/(\pi n\lambda)^2 \approx 10^8$). The transition between these two regimes agrees well with a full model (gray dots) based on Eq. 1. In Fig. 4A we highlight the 19-second ringdown of a 2.46 MHz defect mode, corresponding to $Q = 1.5 \times 10^8$ and $Q \times f = 3.7 \times 10^{14}$ Hz.

Having established near-ideal soft-clamping of uniform nanobeams, we next studied the performance of strain-engineered (tapered) nanobeams. A set of 4 and 7-mm-long tapered PnC nanobeams was fabricated with the length of the taper varied in order to tune the stress at the center of the beam $\sigma(x_c)$ from 2 to 4 GPa (Fig. 2, D and E). We note that for our tapering strategy the width of beam center $w(x_c)$ is fixed, so that the stress is tuned by changing the equilibrium tension T (*20*). Moreover, for each taper length the soft-clamped mode is engineered to be well localized inside the thin taper region by tuning the pitch of unit cells. Measurements of bandgap frequency f_{bg} versus length of the central unit cell length $L_{c,0}$ (parameterizing the taper length) corroborate enhanced stress through correspondence with the theoretical scaling $f_{bg} \propto \sqrt{\sigma(x_c)}/L_{c,0}$ (Fig. 2E).

The Q factors of uniform and tapered PnC nanobeams are compared in Fig. 4. Blue circles correspond to the measurements in Fig. 3G. Red circles are compiled for localized modes of 4-mm-long tapered beams with various peak stresses, corresponding to a bandgap frequency varied from f_{bg} = 1–6 MHz. According to a full model (*20*), $Q(f_{bg})$ should in principle trace out a line of constant $Q \times f \approx 10^{15}$ Hz, exceeding the clamp-free limit of a uniform beam ($Q \times f \propto 1/f$) for sufficiently high frequency. We observe this behavior with an unexplained ~30% reduction, with Q factors exceeding the clamp-free model by a factor of up to three and reaching absolute values high as 3×10^8. Though theoretically this Q should be accessible by soft-clamping alone at lower frequency, our strain-engineering strategy gives access to higher $Q \times f$, reaching a value as high as 8.1×10^{14} Hz for the 3.2 MHz mode of a 4-mm-long device. Higher Q and $Q \times f$ factors were achieved using longer beams (red squares). In Fig. 4A we highlight the 190 s ringdown of a 7-mm-long device excited in its 1.33 MHz defect mode, corresponding to $Q = 8.0 \times 10^8$ and $Q \times f = 1.1 \times 10^{15}$ Hz. We note that at this low damping rate (f/Q ~ 1 mHz), photothermal effects become important. Stroboscopic ringdowns (Fig. 4, A and B) confirm that photothermal damping contributes less than 5% uncertainty (*20*).

Realization of $Q \times f \sim 10^{15}$ in a m~pg mechanical oscillator has numerous intriguing implications. First, such an oscillator is an exquisite force sensor. For example, localized modes of the beam outlined in Fig. 3 are limited by thermal noise to a sensitivity of $\sqrt{8\pi k_B T m f/Q} \approx 3\left(\mathrm{aN}/\sqrt{\mathrm{Hz}}\right)$ at T = 300 K. This value is on par with a typical AFM cantilever operating at 100 times lower frequency and temperature (*22*), creating new opportunities for applications such as high-speed force microscopy (*23*). Of practical importance is that the reported devices also exhibit an exceptionally strong thermal displacement of $\sqrt{k_B T Q/\left(4\pi^3 m f^3\right)} \sim \mathrm{nm}/\sqrt{\mathrm{Hz}}$, accessible by rudimentary detection techniques such as deflectometry. Indeed, their zero-point motion $\sqrt{\hbar Q/\left(2\pi^2 m f^2\right)} \sim \mathrm{pm}/\sqrt{\mathrm{Hz}}$ is orders of magnitude larger than the sensitivity of modern microcavity-based optical interferometers (*24*), offering possibilities in the field of quantum measurement and control (*25*). A fascinating prospect is to use measurement-based feedback to cool such an oscillator to its ground state from room temperature (*26*). A basic requirement is that the oscillator undergo a single oscillation in the thermal decoherence time $\hbar Q/k_B T$. The devices reported are exceptional in this respect, capable of performing $(2\pi Q \times f)/(k_B T/\hbar) > 100$ coherent oscillations at room temperature.

Looking forward, the performance of our devices seems far from exhausted. First, the dilution factors we have achieved are still an order of magnitude below the limit set by the yield stress of Si_3N_4. Our results may thus benefit from more aggressive strain engineering. (For example, Si microbridges have been fabricated with local stresses as high as 7.6 GPa (*14*).) We also emphasize that higher aspect ratios offer a direct route to higher Q. The aspect ratios of our longest beams ($L/h = 3.5 \times 10^5$) appear to be anomalously high for a suspended thin film, including 2D materials (*27*); however, Si_3N_4 membranes with cm-scale dimensions have recently been reported (*28*), hinting at a trend toward more extreme devices. Finally, we note that the source of intrinsic loss in our devices is unknown, but likely due to surface imperfections (*17*). To test this hypothesis, defect-Qs for beams with thicknesses h = 20, 50, and 100 nm were compiled (Fig. 4D). The inferred thickness-dependence of

the intrinsic Q, $Q_0 \approx 6900 \cdot h/100$ nm, is indeed a signature of surface loss, and agrees well in absolute terms with a recent meta-study on Si_3N_4 nanomechanical resonators (*17*). Remarkably, the $Q \propto Q_0/h^2$ scaling of soft-clamped resonators (*8*) preserves the advantage of thinner devices even in the presence of surface loss. It therefore seems appealing to apply our approach to epitaxially-strained crystalline thin films (*29*), which can have 100-fold larger Q_0 at temperatures below 10 K (*30*).

REFERENCES AND NOTES

1. J. Li, Z. Shan, E. Ma, Elastic strain engineering for unprecedented materials properties. *MRS Bull.* **39**, 108–114 (2014). doi:10.1557/mrs.2014.3

2. J. Feng, X. Qian, C.-W. Huang, J. Li, Strain-engineered artificial atom as a broad-spectrum solar energy funnel. *Nat. Photonics* **6**, 866–872 (2012). doi:10.1038/nphoton.2012.285

3. P. Chidambaram, C. Bowen, S. Chakravarthi, C. Machala, R. Wise, Fundamentals of silicon material properties for successful exploitation of strain engineering in modern CMOS manufacturing. *IEEE Trans. Electron Dev.* **53**, 944–964 (2006). doi:10.1109/TED.2006.872912

4. V. B. Braginsky, *Systems with Small Dissipation* (Univ. of Chicago Press, 1985).

5. G. I. González, P. R. Saulson, Brownian motion of a mass suspended by an anelastic wire. *J. Acoust. Soc. Am.* **96**, 207–212 (1994). doi:10.1121/1.410467

6. Q. P. Unterreithmeier, T. Faust, J. P. Kotthaus, Damping of nanomechanical resonators. *Phys. Rev. Lett.* **105**, 027205 (2010). doi:10.1103/PhysRevLett.105.027205 Medline

7. S. Schmid, K. D. Jensen, K. H. Nielsen, A. Boisen, Damping mechanisms in high-Q micro and nanomechanical string resonators. *Phys. Rev. B* **84**, 165307 (2011). doi:10.1103/PhysRevB.84.165307

8. Y. Tsaturyan, A. Barg, E. S. Polzik, A. Schliesser, Ultracoherent nanomechanical resonators via soft clamping and dissipation dilution. *Nat. Nanotechnol.* **12**, 776–783 (2017). doi:10.1038/nnano.2017.101 Medline

9. D. R. Southworth, R. A. Barton, S. S. Verbridge, B. Ilic, A. D. Fefferman, H. G. Craighead, J. M. Parpia, Stress and silicon nitride: A crack in the universal dissipation of glasses. *Phys. Rev. Lett.* **102**, 225503 (2009). doi:10.1103/PhysRevLett.102.225503 Medline

10. D. J. Wilson, C. A. Regal, S. B. Papp, H. J. Kimble, Cavity optomechanics with stoichiometric SiN films. *Phys. Rev. Lett.* **103**, 207204 (2009). doi:10.1103/PhysRevLett.103.207204 Medline

11. S. Chakram, Y. S. Patil, L. Chang, M. Vengalattore, Dissipation in ultrahigh quality factor SiN membrane resonators. *Phys. Rev. Lett.* **112**, 127201 (2014). doi:10.1103/PhysRevLett.112.127201 Medline

12. D. Yu, J. Feng, J. Hone, Elastically strained nanowires and atomic sheets. *MRS Bull.* **39**, 157–162 (2014). doi:10.1557/mrs.2014.6

13. M. Süess, R. Geiger, R. A. Minamisawa, G. Schiefler, J. Frigerio, D. Chrastina, G. Isella, R. Spolenak, J. Faist, H. Sigg, Analysis of enhanced light emission from highly strained germanium microbridges. *Nat. Photonics* **7**, 466–472 (2013). doi:10.1038/nphoton.2013.67

14. R. A. Minamisawa, M. J. Süess, R. Spolenak, J. Faist, C. David, J. Gobrecht, K. K. Bourdelle, H. Sigg, Top-down fabricated silicon nanowires under tensile elastic strain up to 4.5%. *Nat. Commun.* **3**, 1096 (2012). doi:10.1038/ncomms2102 Medline

15. A. Castellanos-Gomez, R. Roldán, E. Cappelluti, M. Buscema, F. Guinea, H. S. J. van der Zant, G. A. Steele, Local strain engineering in atomically thin MoS_2. *Nano Lett.* **13**, 5361–5366 (2013). doi:10.1021/nl402875m Medline

16. P.-L. Yu, T. P. Purdy, C. A. Regal, Control of material damping in high-Q membrane microresonators. *Phys. Rev. Lett.* **108**, 083603 (2012). doi:10.1103/PhysRevLett.108.083603 Medline

17. L. G. Villanueva, S. Schmid, Evidence of surface loss as ubiquitous limiting damping mechanism in SiN micro- and nanomechanical resonators. *Phys. Rev. Lett.* **113**, 227201 (2014). doi:10.1103/PhysRevLett.113.227201 Medline

18. A. H. Ghadimi, D. J. Wilson, T. J. Kippenberg, Radiation and internal loss engineering of high-stress silicon nitride nanobeams. *Nano Lett.* **17**, 3501–3505 (2017). doi:10.1021/acs.nanolett.7b00573 Medline

19. R. Zhang, C. Ti, M. I. Davanço, Y. Ren, V. Aksyuk, Y. Liu, K. Srinivasan, Integrated tuning fork nanocavity optomechanical transducers with high fMQM product and stress-engineered frequency tuning. *Appl. Phys. Lett.* **107**, 131110 (2015). doi:10.1063/1.4932201

20. See supplementary materials.

21. J. Chan, A. H. Safavi-Naeini, J. T. Hill, S. Meenehan, O. Painter, Optimized optomechanical crystal cavity with acoustic radiation shield. *Appl. Phys. Lett.* **101**, 081115 (2012). doi:10.1063/1.4747726

22. M. Poggio, C. L. Degen, H. J. Mamin, D. Rugar, Feedback cooling of a cantilever's fundamental mode below 5 mK. *Phys. Rev. Lett.* **99**, 017201 (2007). doi:10.1103/PhysRevLett.99.017201 Medline

23. M. Poggio, C. L. Degen, Force-detected nuclear magnetic resonance: Recent advances and future challenges. *Nanotechnology* **21**, 342001 (2010). doi:10.1088/0957-4484/21/34/342001 Medline

24. M. Aspelmeyer, T. J. Kippenberg, F. Marquardt, Cavity optomechanics. *Rev. Mod. Phys.* **86**, 1391–1452 (2014). doi:10.1103/RevModPhys.86.1391

25. D. J. Wilson, V. Sudhir, N. Piro, R. Schilling, A. Ghadimi, T. J. Kippenberg, Measurement-based control of a mechanical oscillator at its thermal decoherence rate. *Nature* **524**, 325–329 (2015). doi:10.1038/nature14672 Medline

26. Y.-C. Liu, R.-S. Liu, C.-H. Dong, Y. Li, Q. Gong, Y.-F. Xiao, Cooling mechanical resonators to the quantum ground state from room temperature. *Phys. Rev. A* **91**, 013824 (2015). doi:10.1103/PhysRevA.91.013824

27. R. A. Barton, B. Ilic, A. M. van der Zande, W. S. Whitney, P. L. McEuen, J. M. Parpia, H. G. Craighead, High, size-dependent quality factor in an array of graphene mechanical resonators. *Nano Lett.* **11**, 1232–1236 (2011). doi:10.1021/nl1042227 Medline

28. J. P. Moura, R. A. Norte, J. Guo, C. Schäfermeier, S. Gröblacher, Centimeter-scale suspended photonic crystal mirrors. arXiv:1707.08128 (2017).

29. G. D. Cole, P.-L. Yu, C. Gärtner, K. Siquans, R. Moghadas Nia, J. Schmöle, J. Hoelscher-Obermaier, T. P. Purdy, W. Wieczorek, C. A. Regal, M. Aspelmeyer, Tensile-strained $In_xGa_{1-x}P$ membranes for cavity optomechanics. *Appl. Phys. Lett.* **104**, 201908 (2014). doi:10.1063/1.4879755

30. G. D. Cole, W. Zhang, M. J. Martin, J. Ye, M. Aspelmeyer, Tenfold reduction of Brownian noise in high-reflectivity optical coatings. *Nat. Photonics* **7**, 644–650 (2013). doi:10.1038/nphoton.2013.174

ACKNOWLEDGMENTS

The authors thank Hendrik Schütz and Ehsan Mansouri for valuable contributions during the initial phase of the experiment. **Funding:** This work was supported by the EU Horizon 2020 Research and Innovation Program under grant agreement no. 732894 (FET Proactive HOT) and the SNF Cavity Quantum Optomechanics project (grant no. 163387). M.J.B. is supported by MSCA ETN-OMT (grant no. 722923). T.J.K acknowledges support from ERC AdG (QuREM, grant no. 320966). All samples were

fabricated at the Center for MicroNanoTechnology (CMi) at EPFL. **Author contributions:** Device design and simulation was led by A.H.G. and S.A.F. with early support from R.S.. Devices were fabricated by A.H.G. and M.J.B.. S.A.F. developed the semi-analytical model. All authors contributed to measurements and/or development of the experimental apparatus. Data analysis was led by N.J.E., S.A.F., and D.J.W. with support from A.H.G. and M.J.B.. The manuscript was initially drafted by D.J.W. and S.A.F. with support from N.J.E.. D.J.W., S.A.F., N.J.E., A.H.G., M.J.B., and T.J.K. all participated in editing of the final manuscript and supporting information. D.J.W. and T.J.K. supervised the project. **Competing interests:** None declared. **Data and materials availability:** Data and data analysis code are available through Zonedo at http://dx.doi.org/10.5281/zenodo.1202322. All other data needed to evaluate the conclusions in the paper are present in the paper or the supplementary materials.

SUPPLEMENTARY MATERIALS

www.sciencemag.org/cgi/content/full/science.aar6939/DC1
Supplementary Text
Figs. S1 to S12

8 December 2017; accepted 28 March 2018
Published online 12 April 2018
10.1126/science.aar6939

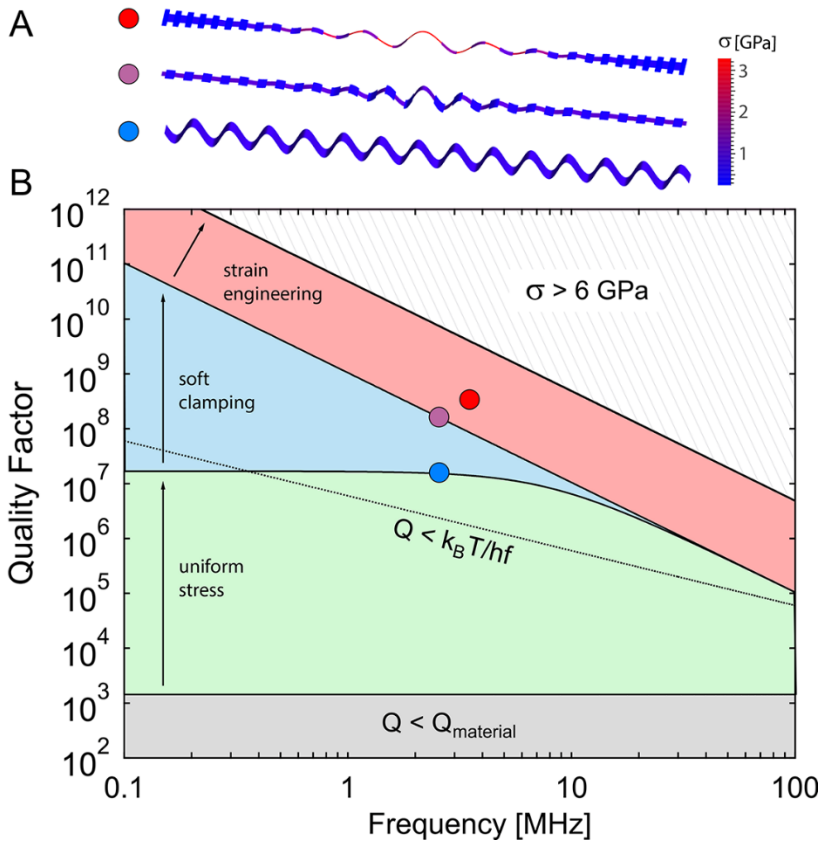

Fig. 1. Ultra-high-*Q* nanobeams through dissipation dilution. (**A**) Mode shapes representing three strategies to enhance the *Q* of a nanobeam via dissipation dilution. From bottom to top: uniform stress, soft-clamping, and geometric strain engineering. Color-coding represents axial stress, σ. (**B**) *Q* versus mode frequency (*f*) accessible for a 20-nm-thick Si_3N_4 nanobeam, following Eq. 3. Gray region: *Q*(*f*) of an unstressed beam, limited by material loss. Green region: *Q*(*f*) of a 3-mm-long uniform beam with $\sigma < 1$ GPa. Blue region: *Q*(*f*) accessible by soft-clamping. Red region: *Q*(*f*) accessible by soft-clamping and strain engineering. Hatched region is forbidden by the material yield strength. Solid circles correspond to measurements described in the main text.

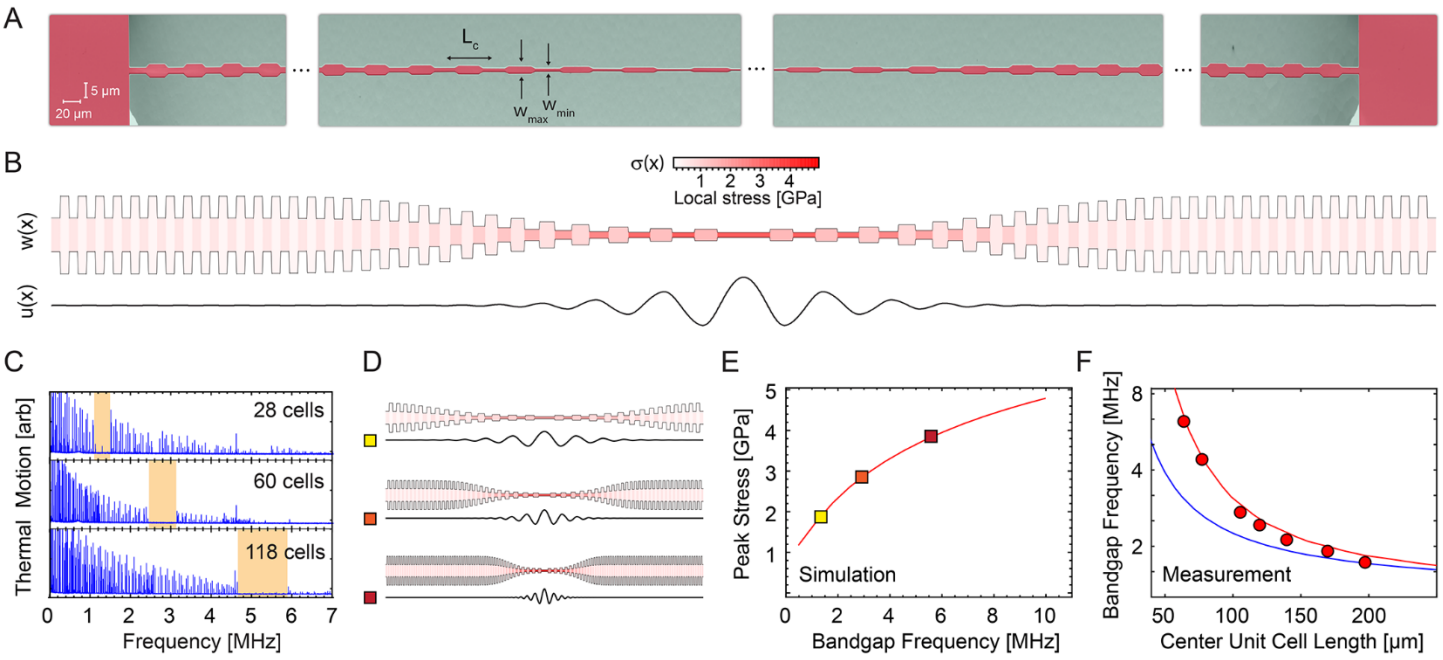

Fig. 2. Strain-engineered 1D phononic crystals. (**A**) Scanning electron micrograph (SEM) of a tapered PnC nanobeam, vertically scaled for perspective. (**B**) Width/stress profile and defect mode shape of a device with 60 unit cells. (**C**) Thermal displacement spectrum of 4-mm-long devices with profiles shown in (**D**). Bandgaps are highlighted in orange. (**E**) Simulation of peak stress versus bandgap frequency f_{bg} for devices shown in (D). (**F**) Measurements of f_{bg} versus length of the central unit cell (parameterizing the taper length). Red and blue lines are models with and without accounting for stress localization, respectively (see text).

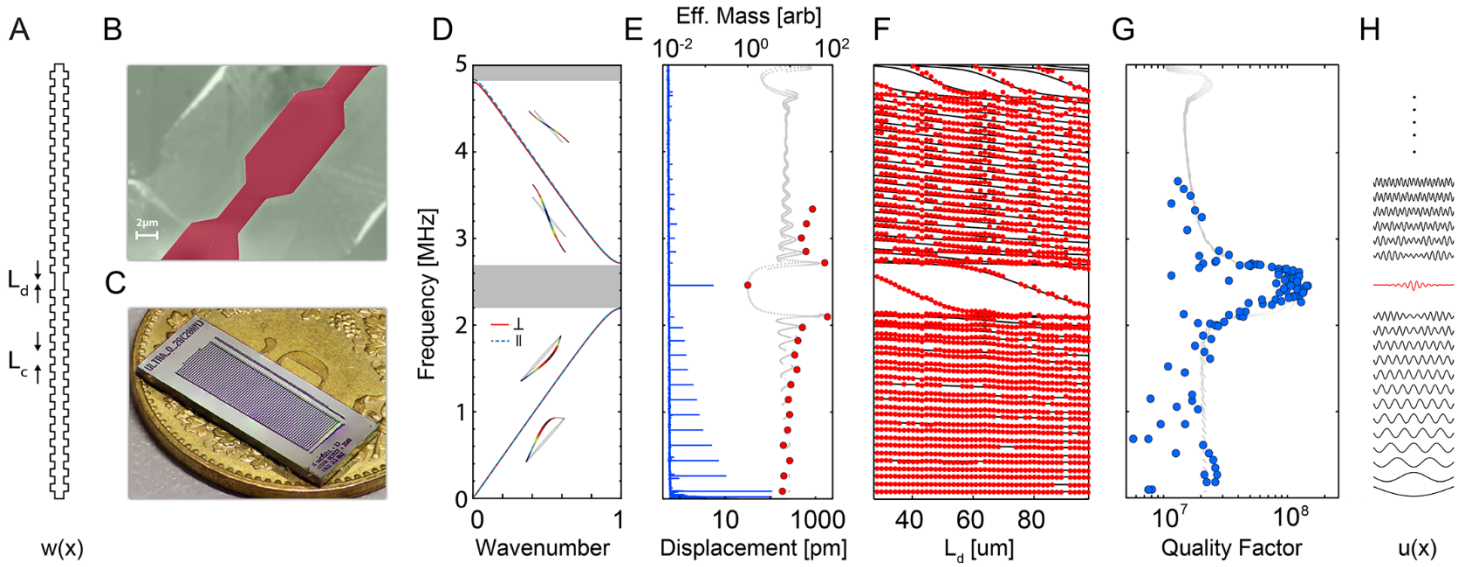

Fig. 3. "Soft-clamped" 1D nanomechanical resonators. (**A**) Schematic of a phononic crystal nanobeam with central defect. See main text for details. (**B**) SEM image of a unit cell. (**C**) Optical image of a sample chip with 76 beams, each with a different defect length. (**D**) Band diagram showing in(∥)- and out(⊥)-of-plane normal modes of a unit cell. (**E**) Displacement spectrum (blue) of a single beam, scaled to the theoretical RMS thermal displacement of the defect mode, $\sqrt{k_B T / m_d (2\pi f)^2}$ ≈ 6 pm. Overlaid are effective mass coefficients m/m_d (red circles) inferred from the area beneath noise peaks. Gray is a model based on modeshapes in (H), used to estimate m_d ≈ 5 pm (*20*). (**F**) Frequency spectra of multiple beams with different defect length. Black lines are a solution to the Euler-Bernoulli equation. (**G**) Compilation of *Q* measurements for a subset of the modes in (F), overlaid with a model based on Eq. 1. (**H**) Modeshapes obtained from the Euler-Bernoulli equation.

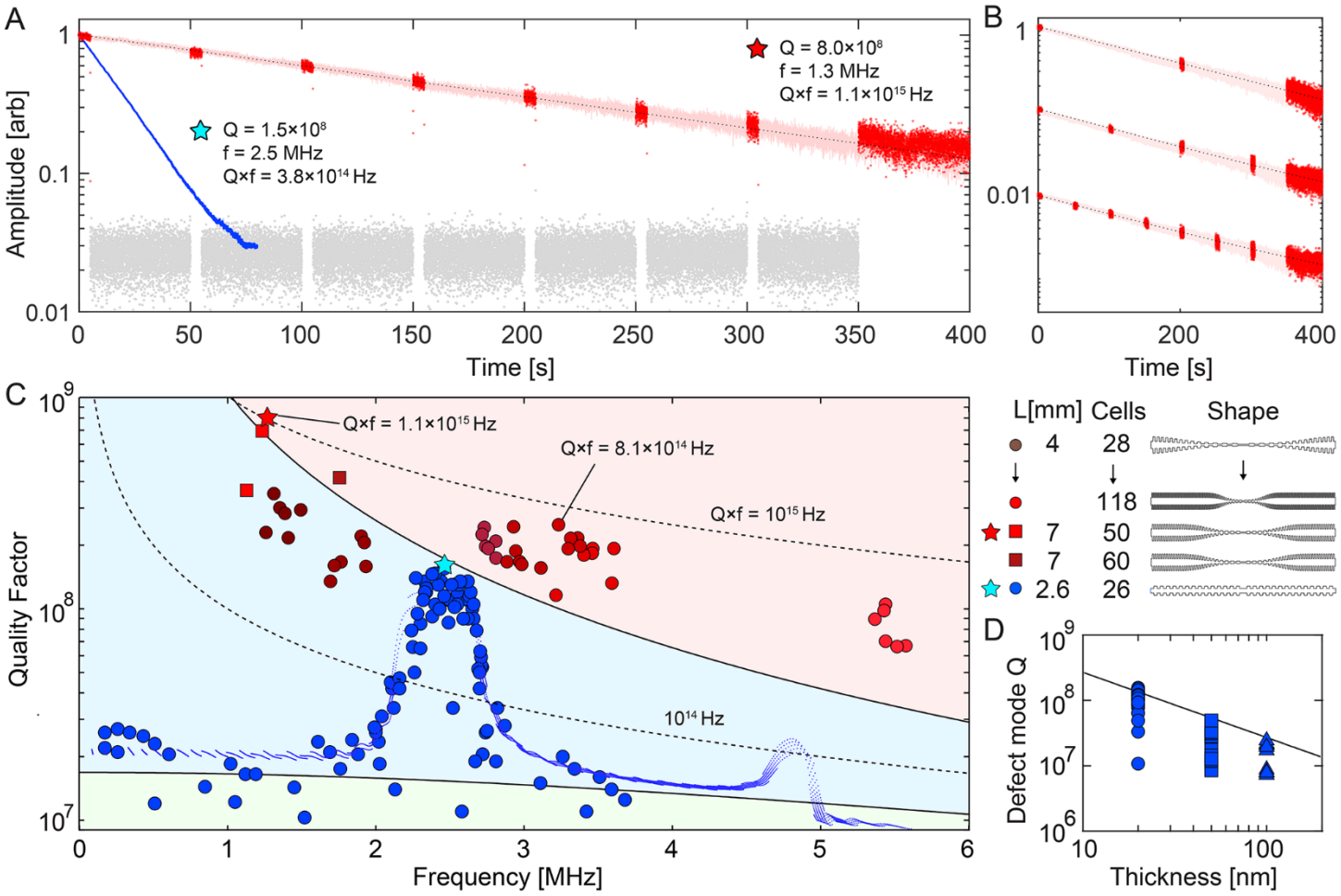

Fig. 4. Enhancing the quality factor of a soft-clamped nanobeam by strain-engineering. (**A**) Interferometric ringdown of a 7-mm-long, 20-nm-thick tapered PnC nanobeam excited in its 1.33 MHz defect mode (pink). Dotted line is an exponential fit with a decay time of 190 s. The inferred Q of 8.0 × 10^8 is indicated by a red star in (C). Overlaid is a stroboscopic ringdown with measurement-on(off) intervals in red(gray). (**B**) Fits to stroboscopic ringdowns with different duty cycles yield the same Q to within 5%, suggesting that photothermal damping is negligible. Also shown in (A) is a ringdown of a uniform PnC nanobeam (cyan star in (C)). (**C**) Q versus mode frequency of PnC nanobeams with different geometries. Blue points correspond to modes of the uniform PnC nanobeam described in Fig. 3. Red points correspond to defect modes of tapered beams. Color groups include the highest five Q factors recorded for different beams. Red lines and blue dots are numerical models based on Eq. 1. (**D**) Compilation of defect mode Q for uniform PnC nanobeams (Fig. 3) of different thickness. Overlaid is a model with $Q_0 = 6900 \cdot h/(100\ \text{nm})$, consistent with surface loss.

Elastic strain engineering for ultralow mechanical dissipation

A. H. Ghadimi, S. A. Fedorov, N. J. Engelsen, M. J. Bereyhi, R. Schilling, D. J. Wilson and T. J. Kippenberg

published online April 12, 2018

Science (print ISSN 0036-8075; online ISSN 1095-9203) is published by the American Association for the Advancement of Science, 1200 New York Avenue NW, Washington, DC 20005.